ASME Journal of Engineering for Gas Turbines and Power
Online journal at:
https://asmedigitalcollection.asme.org/gasturbinespower

Zhaoming Mai
State Key Laboratory of Multiphase Flow in Power Engineering, Xi'an Jiaotong University, Xi'an 710049, China

Yingtao Wu[1]
State Key Laboratory of Multiphase Flow in Power Engineering, Xi'an Jiaotong University, Xi'an 710049, China
e-mail: wuyingtao@xjtu.edu.cn

Chenglong Tang[1]
State Key Laboratory of Multiphase Flow in Power Engineering, Xi'an Jiaotong University, Xi'an 710049, China
e-mail: chenglongtang@mail.xjtu.edu.cn

Wei Wang
State Key Laboratory of Multiphase Flow in Power Engineering, Xi'an Jiaotong University, Xi'an 710049, China;
WFIERI China Faw Corporation Limited, Wu'xi 214063, China

Zuohua Huang
State Key Laboratory of Multiphase Flow in Power Engineering, Xi'an Jiaotong University, Xi'an 710049, China

Understanding the Nonlinear Reactivity Promoting Effect of *n*-Heptane Addition on the Binary Mixture From Low to Intermediate Temperature: A Case of Methane/*n*-Heptane Mixtures

To understand the effect of n*-heptane (NC_7H_{16}) addition on the auto-ignition of methane (CH_4) at low to intermediate temperatures, the ignition delay times (IDTs) of stoichiometric CH_4/NC_7H_{16} blends with varying NC_7H_{16} concentrations were measured at temperatures from 600 to 1000 K, pressures of 20 and 40 bar. Detailed chemical kinetic mechanisms were validated against the newly measured IDTs. Adding NC_7H_{16} in the binary mixture shows a nonlinear promoting effect on the IDTs: micro-addition of NC_7H_{16} can significantly reduce the IDTs of the binary mixture when the NC_7H_{16} is lower than 20%. However, the decrease of the IDTs becomes much slower when further increasing the NC_7H_{16} addition. Affected by the negative temperature coefficient (NTC) behavior of NC_7H_{16}, this nonlinear effect is particularly notable at around 795 K, the low boundary of the NTC region. To reveal the nonlinear reactivity-promoting effect of NC_7H_{16} addition on the binary mixture, reaction flux, ignition sensitivity, rate of production of the key radicals along heat production analyses were conducted. Apart from contributing more $\dot{O}H$ production through the low-temperature chain-branching reaction pathways of NC_7H_{16}, adding NC_7H_{16} also promotes the pre-ignition heat release of the binary mixture. The heat release raises the system temperature and further promotes the mixture ignition, enhancing the nonlinear effect at low temperatures.* [DOI: 10.1115/1.4064148]

Keywords: CH_4/NC_7H_{16} mixture, dual fuel engine, rapid compression machine, ignition delay time, chemical kinetics

1 Introduction

The Compression Ignition (CI) engine still serves as the primary power source of various equipment such as heavy-duty automotive, marine, and power generation [1]. Nonetheless, the widespread utilization of fossil-based diesel fuels contributes to significant carbon dioxide emissions, further intensifying the greenhouse effect. To address this issue, the adoption of low-carbon alternative fuels offers a viable solution that requires minimal modifications to existing systems [2]. Notably, natural gas is a widely utilized substitute fuel [3,4] for its abundant availability worldwide, along with its lower cost compared to traditional liquid fossil fuels [3].

Natural gas exhibits a higher hydrogen-to-carbon ratio and lower carbon number in comparison to gasoline and diesel, resulting in reduced CO_2 emission [4]. Moreover, its lower adiabatic combustion temperature and leaner local equivalence ratio enable natural gas to effectively mitigate NOx and soot emissions simultaneously [5,6]. Furthermore, the high octane number of natural gas permits the utilization of higher compression ratios in natural gas engines, thereby enhancing thermal efficiency [7,8]. Nonetheless, the application of natural gas in CI engines encounters challenges in terms of ignition, particularly under low-temperature conditions. A "dual-fuel" combustion strategy is consequently introduced to address this issue [9–11]. A little amount of pilot diesel is injected during the compression stroke to trigger the ignition of the premixed natural gas mixture by providing a powerful and distributed flame kernel in a short delay [12,13].

The ignition characteristic of diesel and natural gas blends plays a crucial role in dual-fuel engine control and ultimately determines engine performance [13]. For instance, shorter ignition delay can effectively mitigate NOx emissions but generally leads to an extended combustion duration and a reduction in peak combustion

[1]Corresponding authors.

Manuscript received July 12, 2023; final manuscript received November 1, 2023; published online February 8, 2024. Assoc. Editor: Kalyan Kumar Srinivasan.

pressure [14,15]. Nevertheless, it is challenging to precisely regulate the ignition timing in this dual fuel mode due to the reactivity disparity between natural gas and diesel. Consequently, further investigation into the ignition characteristics of natural gas/diesel dual fuel is warranted. Moreover, the integration of computational fluid dynamics with chemical kinetic mechanisms presents an opportunity for cost reduction in engine design and an improved understanding of the internal combustion procedure. The accuracy of the chemical kinetic mechanisms directly influences the quality of simulation results. Therefore, it is essential to develop and validate the accuracy of the chemical kinetic mechanisms for natural gas and diesel blends.

Since both natural gas and diesel are mixtures that contain various complex components, surrogates are commonly employed in theoretical research to simplify this issue [16]. Natural gas typically comprises over 90% volumetric fraction of CH_4 in most gas sources [17], while NC_7H_{16} exhibits a similar cetane number with diesel [18]. Consequently, CH_4 is widely employed as a surrogate for natural gas [19,20], and NC_7H_{16} is commonly employed as a surrogate for diesel [21,22]. Although extensive studies have been conducted on the ignition behaviors of pure fuels, and their surrogates [23–27], limited experimental investigations have been conducted on binary blended mixtures. Liang et al. [28] measured the IDTs for equivalent CH_4 and NC_7H_{16} blends in a shock tube (ST) under 10 atm, 1250 K to 1750 K. They observed a nonlinear influence of CH_4 content on the IDTs of binary mixtures. Schuh et al. [29] investigated the ignition delay for CH_4 and NC_7H_{16} blended fuels under extremely high-pressure conditions (60 and 100 bar, 671 K to 1284 K) using a rapid compression machine (RCM) and ST. They found that the addition of NC_7H_{16} to the CH_4 mixture increases the reactivity of the mixture at low to intermediate temperatures. Gong et al. [30] measured the IDTs of fuel-lean blends of CH_4/NC_7H_{16} at 1241 K to 1825 K and 2.0 bar in an ST. They also found that the effect of NC_7H_{16} addition on IDTs is nonlinear at such high temperature and low pressure. Recently, Zhu et al. [31] studied the ignition delay of the methane CH_4 blended with three different proportions of diesel at 640–1450 K and 6–20 bar. The results revealed that the blended fuel mixture exhibits two ignition stages and typical negative temperature coefficient (NTC) behavior. The promoting capability of diesel to the IDTs is decreasing with the increase of the diesel proportion, resulting in a nonlinear effect on IDTs. However, to the best of the authors' knowledge, there is still limited IDT database for pure CH_4 blended with NC_7H_{16} at low to intermediate temperatures and high pressures. Additional research is imperative to elucidate the intricate mechanisms underlying the nonlinear reactivity promotion resulting from the addition of NC_7H_{16} in the binary mixture from low to intermediate temperature. The manifestation of this nonlinear effect presents challenges in accurately regulating the IDTs of the binary mixtures.

In this study, the new IDTs of binary CH_4/NC_7H_{16} fuels under 600 K to 1000 K, 20 bar, and 40 bar were measured in an RCM. Two commonly used detailed chemical kinetic mechanisms were validated by the measured IDTs. Additionally, chemical kinetics analyses were conducted to shed light on the intricate interaction mechanism occurring upon the addition of micro-NC7H16 to the CH_4/NC_7H_{16} binary mixtures under low to intermediate temperature conditions. These analyses aimed to unveil the underlying mechanism responsible for the nonlinear reactivity promotion effect.

2 Methodology

2.1 Experiment. The IDTs of the CH_4/NC_7H_{16} binary blends were measured using the RCM at Xi'an Jiaotong University. The structural diagram of the RCM setup is shown in Fig. 1, while detailed descriptions can be found in our previous works [32–34]. An overview of the setup is provided in this brief introduction. This RCM includes a high-pressure tank for providing the driving gas, a pneumatic driving chamber, a hydraulic reducer chamber, a compression chamber, and a combustion chamber. The pressure evolution (p) in the combustion chamber is collected by a piezoelectric pressure transducer (Kistler 6125C) coupled with a charge amplifier (Kistler 5018A). The data are recorded at a frequency of 100 kHz by a data collecting card. Temperature evolution is determined based on the adiabatic core hypothesis [35]

$$\int_{T_0}^{T} \frac{\gamma}{\gamma - 1} \frac{dT}{T} = \ln\left(\frac{p}{p_0}\right)$$

in which T_0 is the initial temperature, p_0 is the initial pressure and γ is the temperature-dependent specific heat ratio of the mixture. The end of compression (EOC) pressure (p_c) and temperature (T_c) serve as the characteristic parameters for characterizing the IDT.

The NC_7H_{16} liquid used in this study was sourced from Energy Chemical, China, and has a purity of 99%. The purities of CH_4, oxygen (O_2), nitrogen (N_2), and argon (Ar) used in this study are exceeding 99.999%. N_2 and Ar were employed as the diluent gases in this experiment to provide a wide range of effective T_c (600–1000 K). The prepared reactive mixture and corresponding

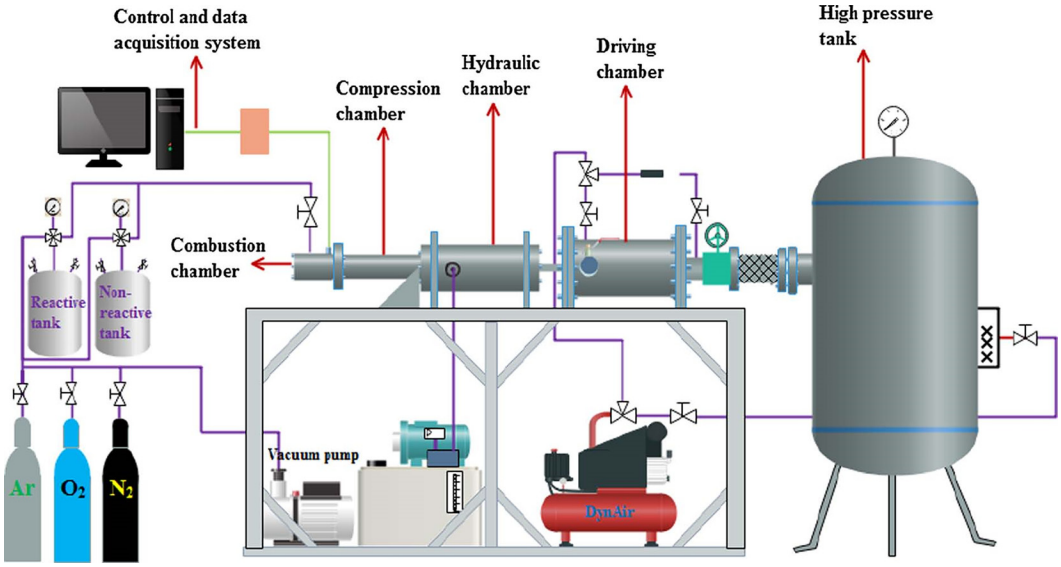

Fig. 1 The structural diagram of the rapid compression machine

Table 1 Compositions of the tested mixtures

		The mole percentage of constituents (%)				
NC_7H_{16} content (%)	ϕ	NC_7H_{16}	CH_4	O_2	N_2/Ar	P_c/bar
0	1.0	0	9.50	19.01	71.49	20, 40
1		0.09	9.04	19.09	71.78	20, 40
2		0.18	8.61	19.16	72.05	20
3		0.25	8.22	19.23	72.30	20, 40
4.5		0.36	7.67	19.32	72.65	20
10		0.68	6.08	19.59	73.65	20, 40
100		1.87	0	20.62	77.51	20

nonreactive mixture (replacing O_2 with equivalent N_2) were separately stored in two stainless-steel tanks. The partial pressure of NC_7H_{16} was maintained below 1/3 of its saturated vapor pressure to prevent condensation. The actual partial pressure of fuel is measured using a digital pressure transducer (OMEGA DPG4000). The composition of the tested mixtures and the corresponding experimental conditions are provided in Table 1.

To ensure the repeatability of the IDTs and minimize measurement error, at least two parallel experiments were conducted for each test condition. Additionally, the nonreactive test at the same condition accounts for the facility-related effects, as depicted in Fig. 2, including the compression process and the heat loss after the EOC. By comparing the reactive and nonreactive pressure histories, potential heat release during compression can be identified. The uncertainties associated with the RCM measurements arise from the initial temperature (±1.1 K), initial pressure (±175 Pa), and mixture composition. By using the independent parameters methodology [36], the uncertainty of T_c is less than 10 K, and the IDT measurements are within ±10%. The detailed calculations of ΔT_c are provided as Supplemental Materials on the ASME Digital Collection.

Figure 2 shows a typical pressure evolution obtained from the RCM experiments. (Additional examples of pressure evolutions are available in Fig. S1 in the Supplemental Materials on the ASME Digital Collection). The instant of EOC is designated as time zero. Both reactive and nonreactive pressure traces exhibit an initial increase before the EOC followed by a slight decrease after the EOC due to the heat loss. These pressure traces are nearly identical before ignition occurs. Subsequently, an obvious two-stage pressure rise was observed, which signifies the characteristic two-stage ignition phenomenon.

The first-stage IDTs are defined as the time interval between time zero and the maximum rate of the first-stage pressure rise during the first stage. The total IDTs, on the other hand, encompass the time interval between time zero and the maximum slope of the pressure trace. Volume history [37] is generated from nonreactive pressure traces by utilizing adiabatic compression and expansion theory. Detailed information regarding the experimental conditions, volume histories, and the corresponding measured IDTs can be found in the Supplemental Materials on the ASME Digital Collection.

2.2 Numerical Simulation. To investigate the mechanism of the nonlinear effect of NC_7H_{16} addition on the ignition of the NC_7H_{16}/CH_4 mixture, chemical kinetic simulations were conducted using the zero-dimensional homogeneous reactor in Chemkin-Pro [38]. The volume history tabulation approach [37] was employed to account for the facility effect on the ignition process in the simulation.

CH_4 is an intermediate product during NC_7H_{16} oxidation, and thus the reaction mechanism for NC_7H_{16} contains the submechanism for CH_4. The detailed chemical kinetic mechanism NUIGMech1.1 [25,26] and LLNL3.1 [39] mechanism are widely utilized for investigating the ignition and combustion processes of NC_7H_{16} [40,41], and have been validated against IDTs measured in ST [28,30,42] and RCM [40,43], as well as data obtained from jet-stirred reactor [44–46] and plug-flow reactor [47].

3 Results and Discussion

3.1 Measured Ignition Delay Times and Mechanism Validation. The total IDTs of CH_4/NC_7H_{16} mixtures with various NC_7H_{16} content at 20 and 40 bar are shown in Fig. 3. The solid symbols represent the measured total IDTs in this study, while the hollow symbols denote data from literature [24,26,48], which have been normalized to the target pressures ($p_c = 20$ bar and 40 bar) using a power law pressure dependence [49]. The line represents the model predicted value using the NUIGMech1.1 mechanism (solid line) and LLNL3.1 mechanism (short dash line).

At $p_c = 20$ bar, typical NTC behavior can be found in the mixture with more than 2% NC_7H_{16} content, which becomes more pronounced for the mixture with higher fractions of NC_7H_{16}. The reactivity of the mixtures increases continuously with increasing NC_7H_{16} content, particularly in the NTC region. In comparison to the IDTs for the 2% NC_7H_{16} case, the IDT is approximately 3 times shorter for the 3% NC_7H_{16} case, 10 times shorter for the 4.5% NC_7H_{16} case, and 40 times shorter for the 10% NC_7H_{16} case, at 20 bar and 770 K. In addition, it can be found that adding NC_7H_{16} to the CH_4 mixture can extend the lower temperature ignition limit of the binary mixture. As the pressure is raised to 40 bar, the mixtures present stronger low-temperature reactivity, resulting in significantly reduced total IDTs. The NTC region of the binary mixture appears at the higher temperature area, and the IDTs exceed the effective measurement time scale of the RCM. Therefore, the measurements at this condition do not exhibit NTC behavior.

Both NUIGMech1.1 and LLNL3.1 mechanisms accurately predict the trends of total IDTs under various conditions, as depicted in Fig. 3. However, NUIGMech1.1 performs better in capturing the NTC behavior of the binary mixtures, whereas LLNL3.1 overestimate the total IDTs in the NTC behavior region for the mixture with fewer NC_7H_{16} content. Furthermore, as shown in Fig. 4, NUIGMech1.1 can also better capture the trends of the first-stage

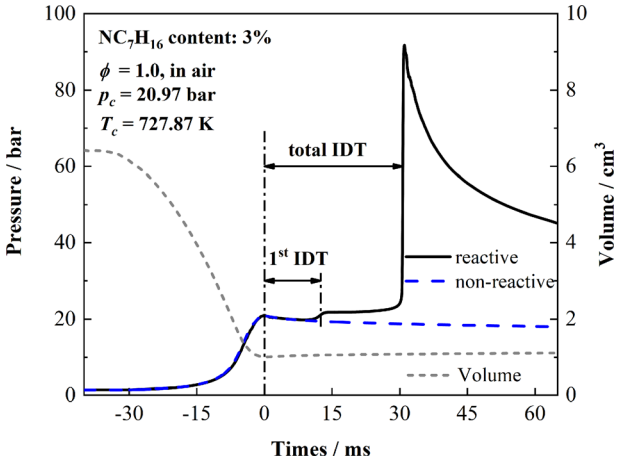

Fig. 2 Typical pressure evolution history for binary mixture measured in XJTU-RCM

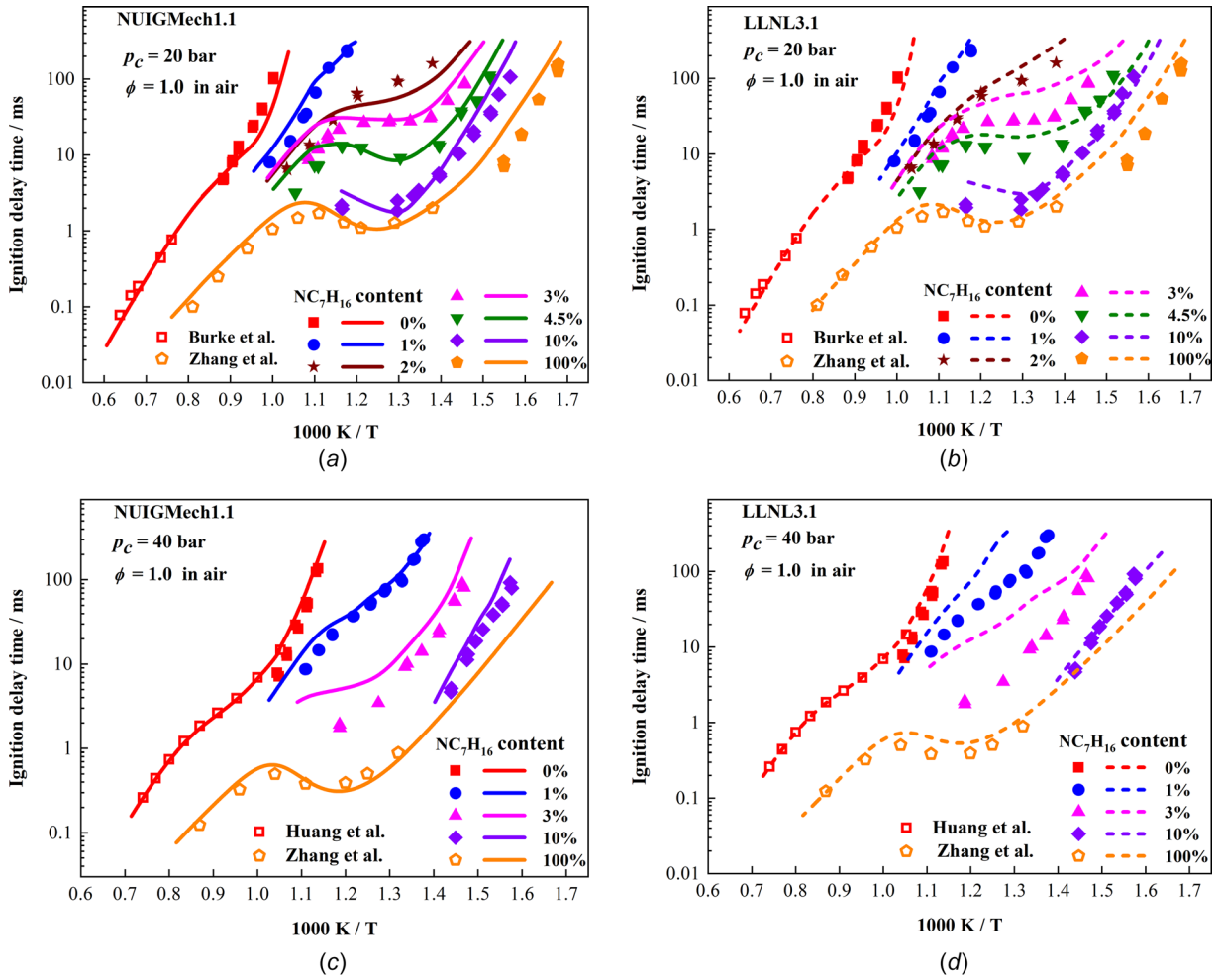

Fig. 3 Total IDT measured (symbols) and model predicted (lines) value for the stoichiometric CH_4/NC_7H_{16} mixture under 20 bar and 40 bar. Hollow symbols are experimental data from Ref. [23,24] for pure CH_4 mixture and from Ref. [26] for pure NC_7H_{16} mixture, Solid and dashed lines are predictions using NUIGMech1.1 [25] and LLNL3.1 [39] mechanism, respectively.

IDTs with temperature and NC_7H_{16} proportion. Consequently, NUIGMech1.1 is selected for further analysis of the chemical kinetic processes during the CH_4/NC_7H_{16} binary mixture auto-ignition.

3.2 Effect of NC_7H_{16} Fraction in Binary Mixture. As mentioned, the addition of NC_7H_{16} to CH_4 has a large impact on the ignition characteristics of the binary mixture. The comparisons of simulated IDTs (see Fig. S2 available in the Supplemental

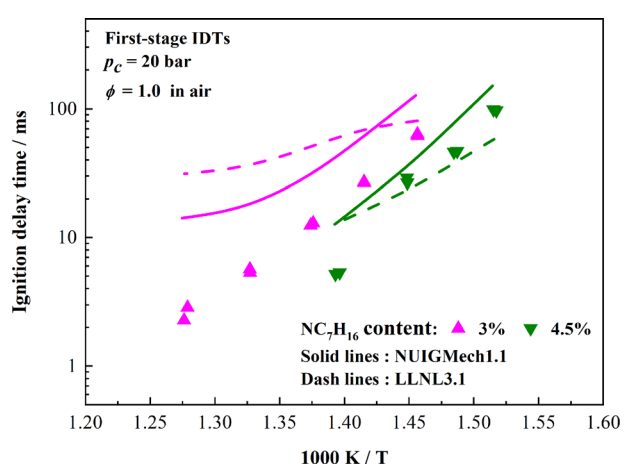

Fig. 4 First-stage IDT measured (symbols) and model predicted (lines) value for stoichiometric CH_4/NC_7H_{16} mixture under 20 bar. Solid and dashed lines are predictions using NUIGMech1.1 [25] and LLNL3.1 [39] mechanisms, respectively.

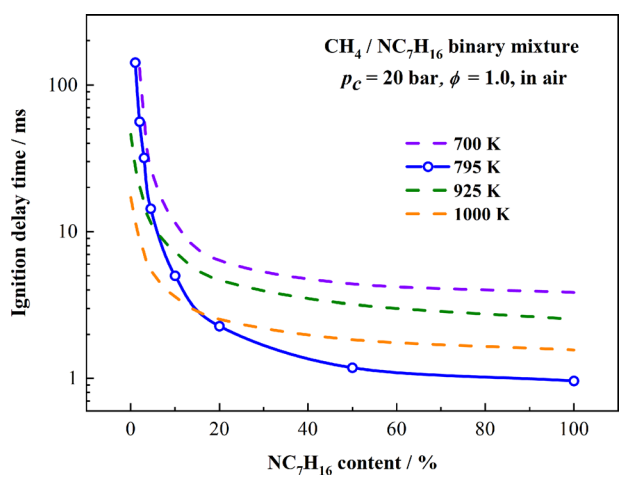

Fig. 5 The evolution of IDTs of stoichiometric CH_4/NC_7H_{16} mixture with various NC_7H_{16} content at temperatures of 700 K, 795 K, 925 K, and 1000 K, under 20 bar, using NUIGMech1.1 mechanism

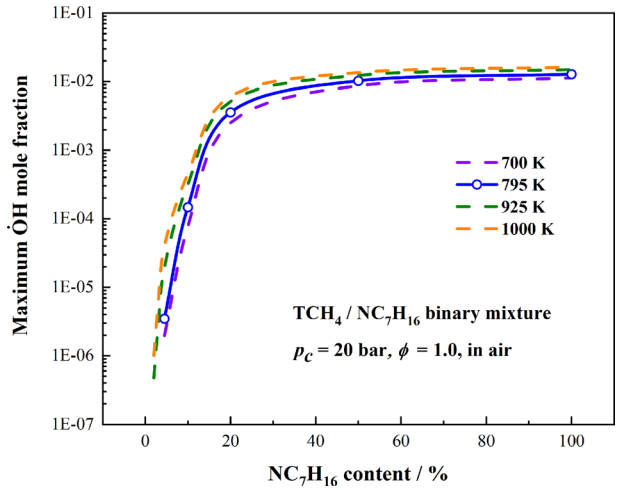

Fig. 6 The evolution of max ȮH mole fraction of TCH_4/NC_7H_{16} mixture with various NC_7H_{16} content at temperatures of 700 K, 795 K, 925 K, and 1000 K, under 20 bar

Materials on the ASME Digital Collection) for the mixture with various NC_7H_{16} content indicated that both the first-stage IDTs and total IDTs decrease as NC_7H_{16} content increases at similar temperature conditions, and the NTC behavior also becomes stronger. The ignition characteristics of the binary mixture gradually approach those of pure NC_7H_{16} mixture as the NC_7H_{16} content increases, and the effect of NC_7H_{16} addition on IDTs is nonlinear.

Figure 5 further illustrates the nonlinear trend of the IDTs with varying NC_7H_{16} content. Four representative temperatures, including 700 K, 795 K, 925 K, and 1000 K, are selected for comparison. These temperatures represent the low temperature, lower temperature limit of the NTC regime, higher temperature limit of the NTC regime, and intermediate temperature under the discussed conditions. It can be observed that there is a significant reduction in IDTs as the NC_7H_{16} content increases from 0% to 20%. When the NC_7H_{16} proportion exceeds 20%, the IDTs of the binary mixture

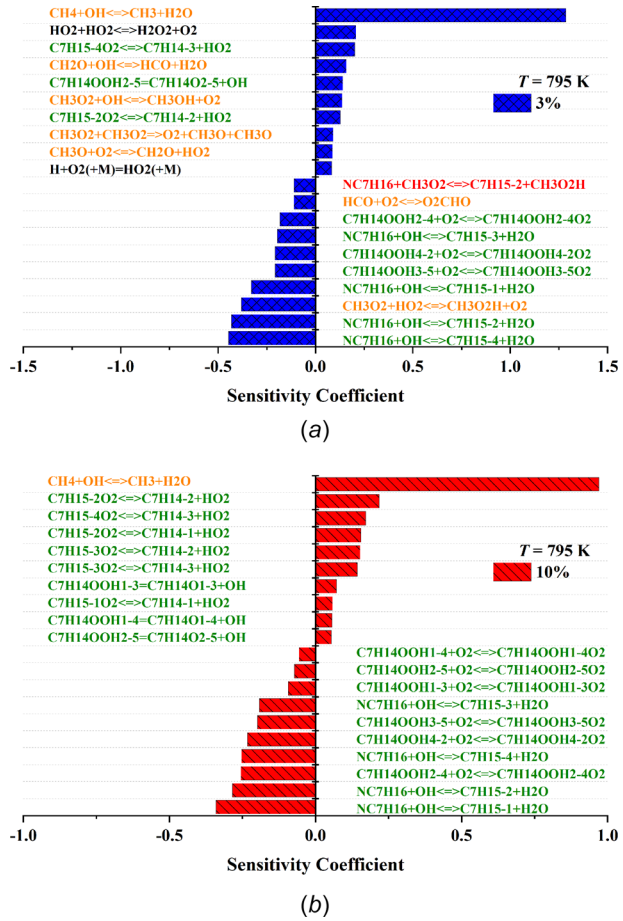

Fig. 8 Sensitivity analyses for first-stage IDT of binary mixture with 3% and 10% NC_7H_{16} content under 20 bar, at (*a*) 795 K and (*b*) 925 K

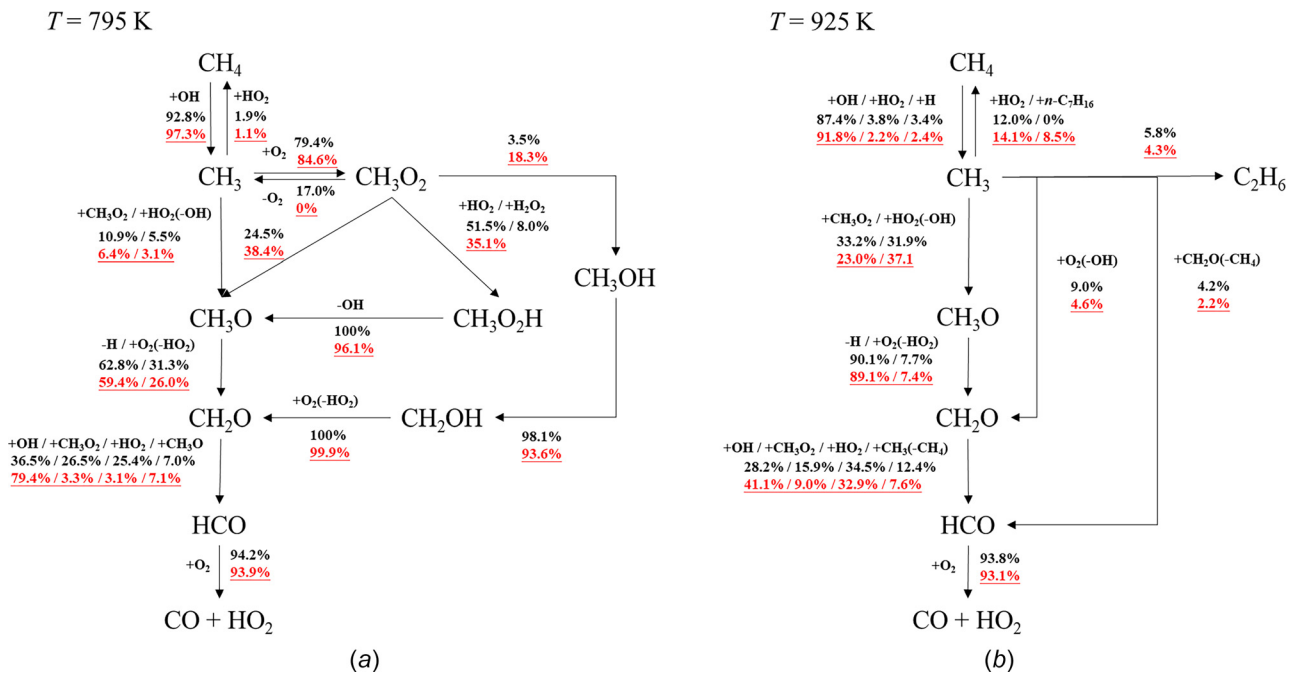

Fig. 7 Reaction flux analysis for CH_4 with 1% (normal) and 10% (underlined) NC_7H_{16} content mixture under 20 bar, at (*a*) 795 K and (*b*) 925 K, where the NC_7H_{16} consumption rates reach 20%

become similar to those of the pure NC_7H_{16} mixture. Notably, the strongest nonlinear effect of NC_7H_{16} content variation on IDTs is observed at $T = 795$ K, which corresponds to the lower temperature limit of the NTC regime for pure NC_7H_{16} mixture.

A hypothetical substance, named "TCH_4", whose thermodynamic properties are identical to CH_4, but do not engage in any reactions, is used to evaluate the effect of NC_7H_{16} addition. The maximum $\dot{O}H$ mole fraction during the auto-ignition of TCH_4/NC_7H_{16} mixtures with varying NC_7H_{16} content is shown in Fig. 6. As the NC_7H_{16} content increases from 0% to 20%, there is a substantial increase in the $\dot{O}H$ mole fraction spanning several orders of magnitude. However, the increase of $\dot{O}H$ mole fraction becomes much slower when the NC_7H_{16} content surpasses 20%. The maximum $\dot{O}H$ mole fraction presents an extremely strong nonlinear growth trend with the NC_7H_{16} content, which is consistent with the effect of NC_7H_{16} addition on the IDTs of the binary mixtures. The $\dot{O}H$ radicals are one of the most important radicals in controlling the mixture ignition. Hence, it can be proposed that the nonlinear introduction of $\dot{O}H$ radicals originating from NC_7H_{16} significantly contributes to the nonlinear effect observed in the IDT of the binary mixture.

3.3 Chemical Kinetic Analyses. Under most temperature conditions, the IDTs exhibit similar nonlinear trends as NC_7H_{16} content increases as illustrated in Fig. 5, and they decrease as the temperature rises. However, there is an extremely strong nonlinear characteristic at 795 K, where the IDTs are even shorter than that at higher temperature conditions when the NC_7H_{16} content is over 5%. In this section, chemical kinetic comparative analyses for CH_4/NC_7H_{16} binary mixture were conducted at 795 K and 925 K, aiming to reveal the mechanism of such strong nonlinear characteristics at 795 K.

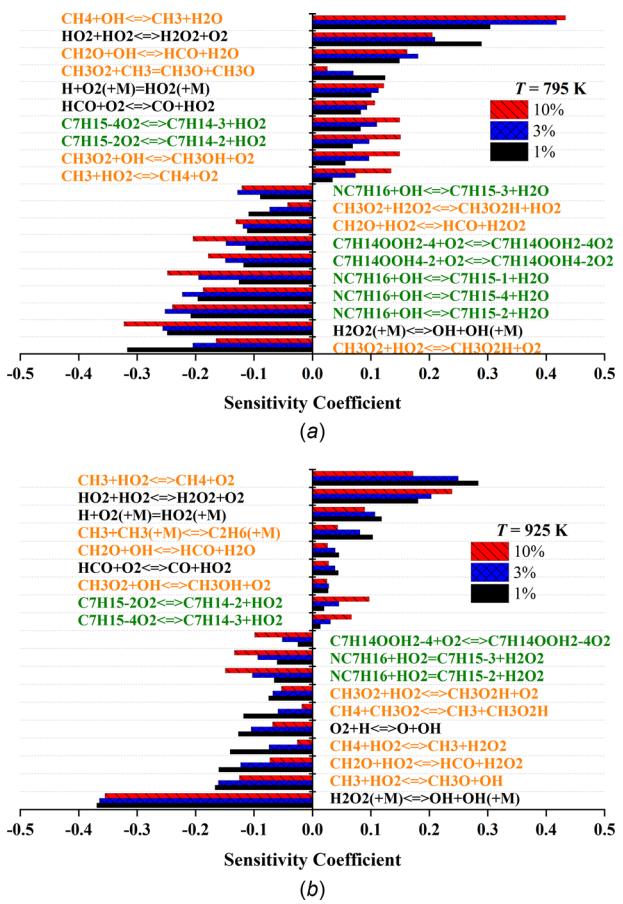

Fig. 9 Sensitivity analyses for total IDT of binary mixture with 1%, 3%, and 10% NC_7H_{16} content under 20 bar, at (*a*) 795 K and (*b*) 925 K

3.3.1 Reaction Flux Analyses for CH_4/NC_7H_{16} Binary Mixture. Figure 7 shows the main reaction pathway of CH_4 when NC_7H_{16} is consumed by 20%. At the relatively lower temperature of 795 K, most of the $\dot{C}H_3$ radicals prefer to combine with O_2 producing $CH_3\dot{O}_2$ radicals. Nearly 60% of $CH_3\dot{O}_2$ radicals react with $H\dot{O}_2$ and H_2O_2 to produce CH_3O_2H, which further dissociates into methoxy ($CH_3\dot{O}$) and releases $\dot{O}H$ radicals. With the increase in NC_7H_{16} content from 1% to 10% at 795 K, the proportion of $CH_3\dot{O}_2$ converting into CH_3O_2H decreases from nearly 60% to 35.1%. So fewer HO_2 radicals transform into $\dot{O}H$ radicals through this pathway. Additionally, the increase of NC_7H_{16} content in the mixture promotes the H-atom abstractions reaction by $\dot{O}H$ radicals from CH_4 and CH_2O.

As the temperature increases to 925 K, most of the $\dot{C}H_3$ radicals directly convert into $CH_3\dot{O}$, CH_2O, and $H\dot{C}O$, rather than combine with O_2. The reaction pathway, $CH_3\dot{O}_2+H\dot{O}_2=>CH_3O_2H=>CH_3\dot{O}+\dot{O}H$ is negligible during CH_4 oxidation. Notably, a portion of $\dot{C}H_3$ reacts with $H\dot{O}_2$ to produce CH_4 or undergoes self-recombines to generate stable C_2H_6 molecules. They are typical chain termination reactions that suppress the reactivity of the mixture. The increase of NC_7H_{16} content at 925 K mainly promotes H-atom abstraction reactions by $\dot{O}H$ radicals for CH_4 and CH_2O.

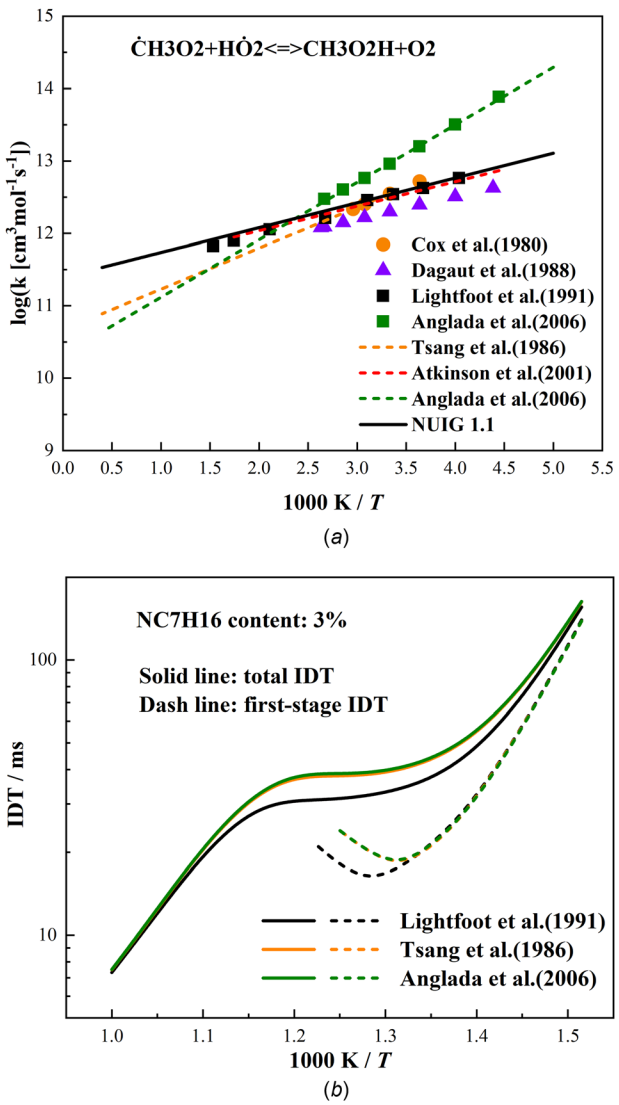

Fig. 10 (*a*) Comparison of the rate constant for $CH_3\dot{O}_2+H\dot{O}_2<=>CH_3O_2H+O_2$ from literature. (*b*) Prediction of IDTs by using different rate constants for $CH_3\dot{O}_2+H\dot{O}_2<=>CH_3O_2H+O_2$.

The main reaction pathways of NC_7H_{16} are also presented in Fig. S3 available in the Supplemental Materials on the ASME Digital Collection during its consumption rate reaches 20% respectively at 20 bar, 795 K, and 925 K. The increase of NC_7H_{16} content in the mixture primarily elevates the proportion of the H-atom abstraction from NC_7H_{16} by $\dot{O}H$ radicals at both 795 K and 925 K. Specifically, $CH_3\dot{O}_2$ and $\dot{C}H_3$ radicals participate in the H-atom abstraction reaction to consume NC_7H_{16} under 1% NC_7H_{16} content conditions. As the temperature increases from 795 K to 925 K, the proportion of the low-temperature oxidation pathway (the secondary-O_2 reaction) reduces, which suppresses the low-temperature reactivity of NC_7H_{16}.

3.3.2 Brute-Force Sensitivity Analyses for the Ignition Delay Times. To further investigate the dominant elementary steps in deciding the reactivity, brute-force sensitivity analyses under the premise of adiabatic conditions were conducted for CH_4/NC_7H_{16} mixture with 1%, 3%, and 10% NC_7H_{16} content at 20 bar and 795 K and 925 K. The sensitivity coefficient for IDTs of the reaction is defined as

$$S = \log(\tau_2/\tau_{0.5})/\log(2/0.5)$$

where τ_2 and $\tau_{0.5}$ are the IDTs (total IDTs or first-stage IDTs) computed with the rate constant multiplied or divided by two, respectively. The reaction with a positive sensitivity coefficient extends the IDT and suppresses the system reactivity, while the reaction with a negative coefficient shortens the IDT and promotes the system reactivity.

The first-stage IDTs mainly occur at relatively lower temperatures ($T = 795$ K, for example) and NC_7H_{16} content higher than 3%. According to Fig. 8, The competition between CH_4 and NC_7H_{16} for $\dot{O}H$ radicals dominates the first-stage ignition process of the binary mixture for both 3% and 10% conditions, and the reactivity is mainly promoted by NC_7H_{16} low-temperature oxidation reactions. The CH_4 in the mixture suppresses the low-temperature reactivity of NC_7H_{16} and extends the first-stage IDT. When the NC_7H_{16} content is below 3%, the suppressed effect of the CH_4-relevant reaction becomes more obvious.

Based on the sensitivity analyses shown in Fig. 9, at the relatively lower temperature of 795 K, the competition between CH_4 and NC_7H_{16} for $\dot{O}H$ radicals also dominates the total IDTs of the binary mixture for all three different NC_7H_{16} content mixtures. The subsequent secondary O_2-addition to the hydroperoxyl-alkyl radicals of NC_7H_{16} also strongly promotes reactivity. For higher NC_7H_{16} content (10%) mixtures, the most reactivity-promoting reaction is $H_2O_2(+M)<=>\dot{O}H+\dot{O}H(+M)$, while it transforms into $CH_3\dot{O}_2+H\dot{O}_2<=>CH_3O_2H+O_2$ at extremely low NC_7H_{16} content (1%) conditions. The further dissociation reaction of CH_3O_2H produces $\dot{O}H$ radicals, which accelerate fuel consumption. Generally, $\dot{O}H$-relevant reactions exhibit large sensitivity coefficients and control the reactivity of binary mixture at low-temperature conditions.

As the temperature increases to 975 K, the chain termination reaction, $\dot{C}H_3+H\dot{O}_2<=>CH_4+O_2$, exhibits the largest sensitivity coefficient, inhibiting reactivity, typically at low NC_7H_{16} content (1%) conditions. The self-recombination reaction of $H\dot{O}_2$ and $\dot{C}H_3$ to produce stable species, H_2O_2 and C_2H_6, also significantly inhibits the reaction. However, the reactions of $H\dot{O}_2$ radicals abstracting

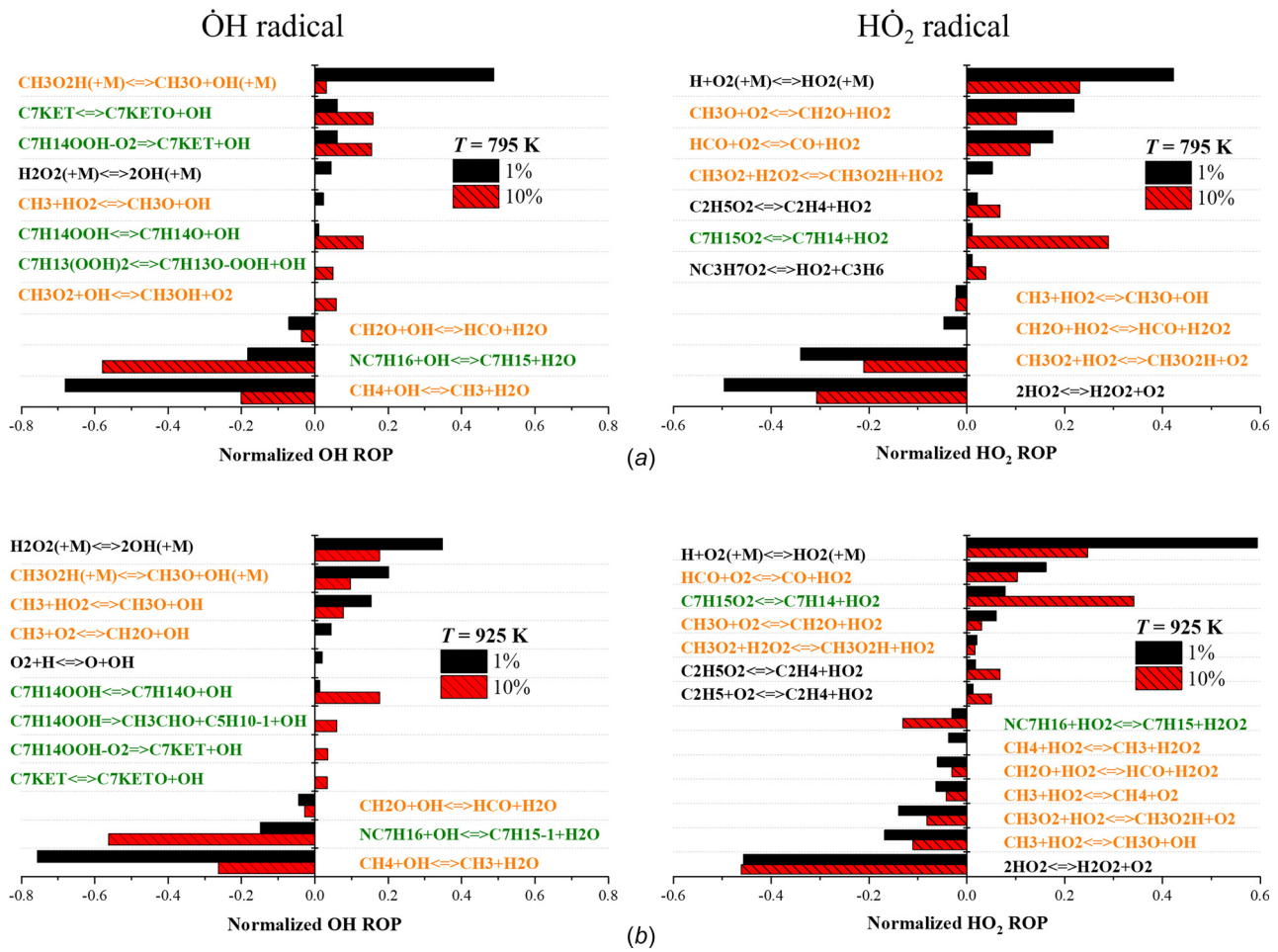

Fig. 11 Normalized ROP analysis of $\dot{O}H$ and $H\dot{O}_2$ radicals in the stoichiometric binary mixture with 1% and 10% NC_7H_{16} content under 20 bar at 795 K, and 925 K, while the NC_7H_{16} consumption rate reaches 20%

H-atom from NC_7H_{16}, CH_4, and CH_2O show higher sensitivity at this temperature. These reactions produce H_2O_2, which further dissociates into two $\dot{O}H$ radicals, greatly promoting fuel consumption. At this temperature, the $H\dot{O}_2$-relevant reactions control the reactivity of the binary mixture and exhibit large sensitivity coefficients.

The reaction of $CH_3\dot{O}_2+H\dot{O}_2<=>CH_3O_2H+O_2$ is found to exhibit higher sensitivity to the IDTs of the binary mixture than that for pure fuels [40,50,51] under low NC_7H_{16} content ($\leq$10%) and low-temperature conditions. It is also involved in the main pathway for generating $\dot{O}H$ radicals: $CH_3\dot{O}_2+H\dot{O}_2=>CH_3O_2H=>CH_3\dot{O}+\dot{O}H$. The rate constant adopted in NUIGMech1.1 is fitted according to the measurements by Lightfoot et al. [52]. It is found to be 2 - 4 times higher than the rate constants fitted from calculation results with multiconfiguration self-consistent field and complete active space self-consistent field method by Anglada et al. [53] and that used by Tsang et al. [54] at the temperature from 600 K to 1000 K as shown in Fig. 10(*a*). Figure 10(*b*) presents the calculated IDTs using the different rate constants for $CH_3\dot{O}_2+H\dot{O}_2<=>CH_3O_2H+O_2$ from Lightfoot et al. [51], Anglada et al. [53] and Tsang et al. [54]. The results show that the difference in rate constants for $CH_3\dot{O}_2+H\dot{O}_2<=>CH_3O_2H+O_2$ can lead to approximately 15%–20% variation of the IDTs in the NTC region. Further investigations by experiments and high levels of theory are required to improve the prediction.

3.3.3 Rate of Production Analysis of $\dot{O}H$ and $H\dot{O}_2$ Radicals. As mentioned before, the interaction between NC_7H_{16} and CH_4 is mainly through $\dot{O}H$ and $H\dot{O}_2$ radicals. Thus, the rate of production (ROP) analysis of $\dot{O}H$ and $H\dot{O}_2$ radicals at 795 K and 925 K, 20 bar, under 20% NC_7H_{16} consumption instant is conducted and shown in Fig. 11. At the relatively lower temperature of 795 K, the $\dot{O}H$ radicals are primarily provided through the reaction $CH_3O_2H(+M)<=>CH_3\dot{O}+\dot{O}H(+M)$ at 1% NC_7H_{16} content condition and mainly consumed by H-atom abstraction reaction of CH_4. For the $H\dot{O}_2$ radicals, $CH_3\dot{O}_2+H\dot{O}_2<=>CH_3O_2H+O_2$ is an important reaction that consumes $H\dot{O}_2$ and provides CH_3O_2H. The flux of $CH_3\dot{O}_2+H\dot{O}_2=>CH_3O_2H=>CH_3\dot{O}+\dot{O}H$ is the major pathway to convert $H\dot{O}_2$ radicals into more active $\dot{O}H$ radicals promoting the reactivity. When the NC_7H_{16} content increases to 10%, the $\dot{O}H$ radicals are mainly generated from the low-temperature oxidation of NC_7H_{16}.

As the temperature increases to 925 K, the $\dot{O}H$ radical is mainly produced through the dissociation reaction of H_2O_2, which primarily arises from the self-recombination of $H\dot{O}_2$ radicals, and H-atom abstraction by $H\dot{O}_2$ radicals from NC_7H_{16}, CH_4, and CH_2O. The reaction pathway of $H\dot{O}_2=>H_2O_2=>\dot{O}H$ becomes the major pathway for converting $H\dot{O}_2$ radicals into more active $\dot{O}H$ radicals. On the other hand, the CH_4-relevant reaction pathways such as $CH_3\dot{O}_2+H\dot{O}_2=>CH_3O_2H=>CH_3\dot{O}+\dot{O}H$ and $CH_3+H\dot{O}_2<=>CH_3\dot{O}+\dot{O}H$ also play an important role in consuming $H\dot{O}_2$ and producing $\dot{O}H$ radicals for both 1% and 10% NC_7H_{16} content mixture. Production of $\dot{O}H$ radicals from the low-temperature reactions of NC_7H_{16} decreases at this temperature.

Figure 12 provides insight into the development of key species for the binary mixture with 1% and 10% NC_7H_{16} contents at 20 bar, 795 K, and 925 K. The start of NC_7H_{16} consumption generally occurs earlier than that of CH_4, which arises initial radicals pool. The initial oxidation of NC_7H_{16} can sharply improve the $\dot{O}H$ radicals' mole fraction in the system, which promotes the binary mixture ignition.

Owing to the low-temperature oxidation characteristic of NC_7H_{16}, increasing NC_7H_{16} content at 795 K can significantly increase the concentration of $\dot{O}H$ radicals and promote the reactivity of the binary mixture. However, at the intermediate temperature of 925 K, the low-temperature reactivity of the NC_7H_{16} is suppressed, resulting in a smaller variation of the $\dot{O}H$ radicals' mole fraction as NC_7H_{16} content increases. Thus, the NC_7H_{16} content presents less effect on IDTs of the binary mixture. This is a reason for a stronger nonlinear behavior observed at 795 K than at 925 K.

3.3.4 Heat Release Analysis for Main Reactions. The consumption of NC_7H_{16} is earlier than that of CH_4, and heat release during NC_7H_{16} oxidation can affect the ignition process of the CH_4 as shown in Fig. 12. Hence, the effect of micro-NC7H16 addition on the CH_4 mixture should also be investigated thermodynamically. Figure 13 provides insight into the major endothermic and exothermic reactions during the consumption of NC_7H_{16} up to 20%, at 795 K and 925 K, 20 bar.

At the relatively lower temperature of 795 K, the CH_4-relevant reactions, such as $CH_3+O_2(+M)<=>CH_3\dot{O}_2(+M)$, $CH_3\dot{O}_2+H\dot{O}_2<=>CH_3O_2H+O_2$, and $CH_4+H\dot{O}_2<=>CH_3+O_2$ are responsible for the main heat release under the 1% NC_7H_{16} condition. When the NC_7H_{16} content increases to 10%, the heat production rates are almost two orders of magnitude higher compared to the 1% NC_7H_{16} condition. On the one hand, the NC_7H_{16}-relevant reactions, including the H-atom abstraction and O_2-addition reactions, contribute to a significant heat release rate at this condition. Therefore, increasing the proportion of NC_7H_{16} can sharply promote the heat release from the NC_7H_{16} oxidation process. On the other hand, low-temperature oxidation of NC_7H_{16} generates a massive of $\dot{O}H$ and $H\dot{O}_2$ radicals, which participate in the CH_4-relevant reactions, such as $CH_4+\dot{O}H<=>\dot{C}H_3+H_2O$, $CH_3\dot{O}_2+H\dot{O}_2<=>CH_3O_2H+O_2$, etc. These reactions also contribute to major exothermic reactions in this condition. As a consequence, the inclusion of a higher fraction of NC_7H_{16} leads to a substantial increase in the system temperature during the first-stage consumption of NC_7H_{16}, as Fig. 12 shows. As the temperature approaches the initial dissociation temperature of H_2O_2 (approximately 1000 K)

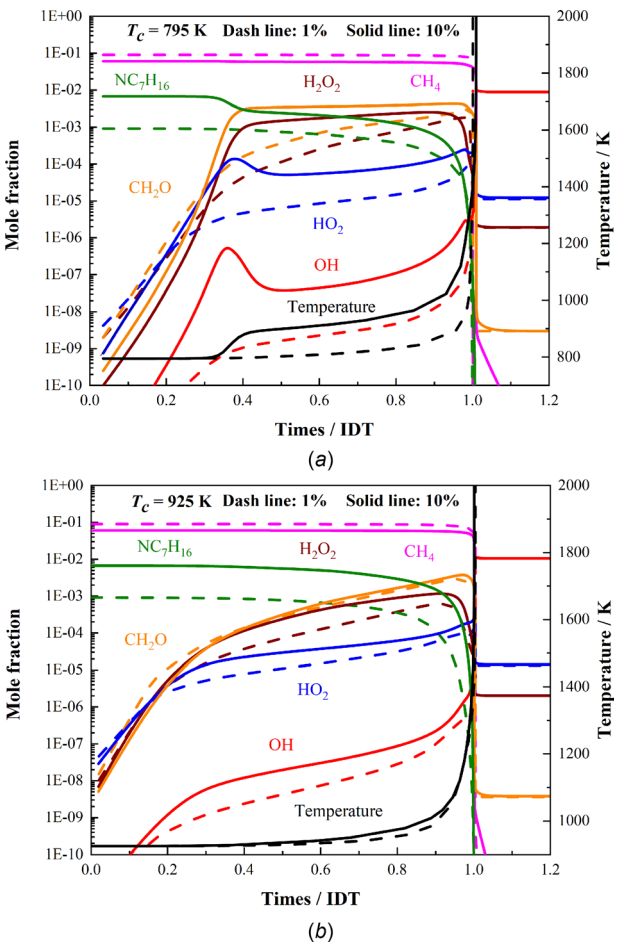

Fig. 12 Evolution of key species and temperature of the stoichiometric binary mixture with 1%, and 10% NC_7H_{16} content under 20 bar, at (*a*) 795 K and (*b*) 925 K with the normalization time

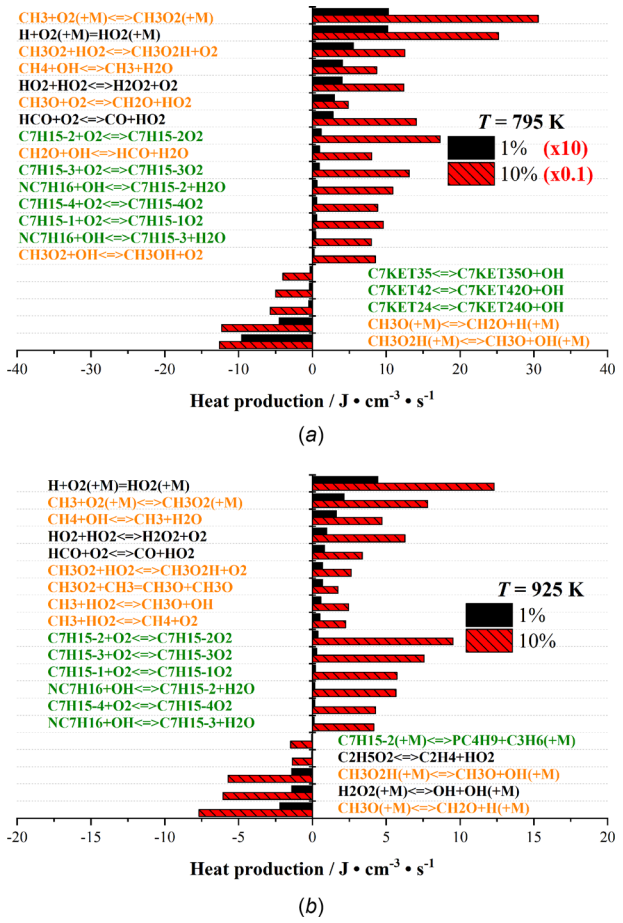

Fig. 13 Major endothermic and exothermic reactions of mixture with 1% and 10% NC_7H_{16} content at 20% NC_7H_{16} consumption. Under 20 bar, at (*a*) 795 K and (*b*) 925 K.

[55], a large amount of $\dot{O}H$ radicals is produced, thereby accelerating the ignition process of the binary mixture.

The effect of NC_7H_{16} addition on the heat production at 925 K is less than that at 925 K. On one hand, the competition between the low-temperature and intermediate-temperature reactions reduces the reactivity of NC_7H_{16} and suppresses heat release during NC_7H_{16} oxidation. On the other hand, the major exothermic reaction, $\dot{C}H_3+O_2(+M)<=>CH_3\dot{O}_2(+M)$ and $CH_3\dot{O}_2+H\dot{O}_2<=>CH_3O_2H+O_2$, constitute a smaller proportion of the CH_4 consumption (as shown in Fig. 7), leading to a slower heat release rate. This is another reason for a stronger nonlinear behavior observed at 795 K than at 925 K.

4 Conclusions

In this study, IDTs for binary mixtures of CH_4 and NC_7H_{16} at various blending ratios are measured under 600 to 1000 K, 20 bar, and 40 bar. The effect of NC_7H_{16} addition on IDTs shows nonlinear characteristics, micro-addition of NC_7H_{16} can significantly reduce the IDTs of the binary mixture when the NC_7H_{16} is lower than 20%. The nonlinear characteristic is particularly notable at around 795 K, corresponding to the lower boundary of the NTC region of pure NC_7H_{16}. And that mainly originated from the NTC behavior of NC_7H_{16}.

From the perspective of reaction pathways, at 795 K, the most important source of $\dot{O}H$ radicals is the reaction pathway of $CH_3\dot{O}_2+H\dot{O}_2=>CH_3O_2H=>CH_3\dot{O}+\dot{O}H$ at extremely low NC_7H_{16} content conditions. It transforms into the low-temperature chain branching reactions of NC_7H_{16} as the NC_7H_{16} content increases. That accelerates both the first stage and total ignition of the binary mixture. However, at higher temperatures of 925 K, the reaction pathway of $H\dot{O}_2=>H_2O_2=>\dot{O}H$ becomes the major source of $\dot{O}H$ radicals for both 1% and 10% NC_7H_{16} content conditions. The influence of NC_7H_{16} content on the $\dot{O}H$ radicals is less than that at 795 K because the low-temperature oxidation pathway is suppressed in the NTC region.

From the perspective of heat production, the influence of NC_7H_{16} proportion on heat production is greater at 795 K compared to 925 K. On the one hand, the low-temperature reaction of NC_7H_{16} can provide a large amount of heat at 795 K. On the other hand, more $\dot{O}H$ radicals provided through the low-temperature oxidation of NC_7H_{16} accelerate CH_4 consumption and promote the heat release from the CH_4-relevant reactions at 795 K. The greater heart release raises the temperature earlier promotes the binary mixture ignition and strengthens the nonlinear characteristics at 795 K than that at 925 K.

Funding Data

- National Natural Science Foundation of China (Grant Nos. 52206168 and 52236001; Funder ID: 10.13039/501100001809).
- Natural Science Basic Research Program of Shanxi (Grant No. 2022JQ-470; Funder ID: 10.13039/501100007128).
- State Key Laboratory of Automotive Safety and Energy (Grant No. KFZ2205; Funder ID: 10.13039/501100011283).

Data Availability Statement

The authors attest that all data for this study are included in the paper.

References

[1] Reitz, R. D., and Duraisamy, G., 2015, "Review of High Efficiency and Clean Reactivity Controlled Compression Ignition (RCCI) Combustion in Internal Combustion Engines," Prog. Energy Combust. Sci., **46**, pp. 12–71.
[2] Bae, C., and Kim, J., 2017, "Alternative Fuels for Internal Combustion Engines," Proc. Combust. Inst., **36**(3), pp. 3389–3413.
[3] Korakianitis, T., Namasivayam, A. M., and Crookes, R. J., 2011, "Natural-Gas Fueled Spark-Ignition (SI) and Compression-Ignition (CI) Engine Performance and Emissions," Prog. Energy Combust. Sci., **37**(1), pp. 89–112.
[4] Wei, L., and Geng, P., 2016, "A Review on Natural Gas/Diesel Dual Fuel Combustion, Emissions and Performance," Fuel Process. Technol., **142**, pp. 264–278.
[5] Huang, H., Lv, D., Zhu, J., Zhu, Z., Chen, Y., Pan, Y., and Pan, M., 2019, "Development of a New Reduced Diesel/Natural Gas Mechanism for Dual-Fuel Engine Combustion and Emission Prediction," Fuel, **236**, pp. 30–42.
[6] Chen, Y. J., Zhu, Z., Chen, Y. J., Huang, H. Z., Zhu, Z. J., Lv, D. L., Pan, M. Z., and Guo, X. Y., 2020, "Study of Injection Pressure Couple With EGR on Combustion Performance and Emissions of Natural Gas-Diesel Dual-Fuel Engine," Fuel, **261**, p. 116409.
[7] Akansu, S., 2004, "Internal Combustion Engines Fueled by Natural Gas-Hydrogen Mixtures," Int. J. Hydrogen Energy, **29**(14), pp. 1527–1539.
[8] Papagiannakis, R. G., Rakopoulos, C. D., Hountalas, D. T., and Rakopoulos, D. C., 2010, "Emission Characteristics of High Speed, Dual Fuel, Compression Ignition Engine Operating in a Wide Range of Natural Gas/Diesel Fuel Proportions," Fuel, **89**(7), pp. 1397–1406.
[9] Chiara, F., and Canova, M., 2009, "Mixed-Mode Homogeneous Charge Compression Ignition—Direct Injection Combustion on Common Rail Diesel Engines: An Experimental Characterization," Int. J. Energy Res., **10**(2), pp. 81–96.
[10] Rapp, V. H., Cannella, W. J., Chen, J. Y., and Dibble, R. W., 2013, "Predicting Fuel Performance for Future HCCI Engines," Combust. Sci. Technol., **185**(5), pp. 735–748.
[11] d'Ambrosio, S., and Ferrari, A., 2015, "Effects of Exhaust Gas Recirculation in Diesel Engines Featuring Late PCCI Type Combustion Strategies," Energy Convers. Manag., **105**, pp. 1269–1280.
[12] Paul, A., Panua, R. S., Debroy, D., and Bose, P. K., 2014, "Effect of Compressed Natural Gas Dual Fuel Operation With Diesel and Pongamia Pinnata Methyl Ester (PPME) as Pilot Fuels on Performance and Emission Characteristics of a CI (Compression Ignition) Engine," Energy, **68**, pp. 495–509.
[13] Srna, A., Bolla, M., Wright, Y. M., Herrmann, K., Bombach, R., Pandurangi, S. S., Boulouchos, K., and Bruneaux, G., 2019, "Effect of Methane on Pilot-Fuel Auto-Ignition in Dual-Fuel Engines," Proc. Combust. Inst., **37**(4), pp. 4741–4749.
[14] Lu, X., Han, D., and Huang, Z., 2011, "Fuel Design and Management for the Control of Advanced Compression-Ignition Combustion Modes," Prog. Energy Combust. Sci., **37**(6), pp. 741–783.
[15] Musculus, M. P. B., Miles, P. C., and Pickett, L. M., 2013, "Conceptual Models for Partially Premixed Low-Temperature Diesel Combustion," Prog. Energy Combust. Sci., **39**(2–3), pp. 246–283.
[16] Li, M., Zhang, Q., Liu, X., Ma, Y., and Zheng, Q., 2018, "Soot Emission Prediction in Pilot Ignited Direct Injection Natural Gas Engine Based on n-Heptane/Toluene/Methane/PAH Mechanism," Energy, **163**, pp. 660–681.

[17] Petersen, E. L., Hall, J. M., Smith, S. D., de Vries, J., Amadio, A. R., and Crofton, M. W., 2007, "Ignition of Lean Methane-Based Fuel Blends at Gas Turbine Pressures," ASME J. Eng. Gas Turbines Power, **129**(4), pp. 937–944.
[18] Herzler, J., Jerig, L., and Roth, P., 2005, "Shock Tube Study of the Ignition of Lean n-Heptane/Air Mixtures at Intermediate Temperatures and High Pressures," Proc. Combust. Inst., **30**(1), pp. 1147–1153.
[19] Sanli, A., Ylmaz, I. T., and Gümüş, M., 2020, "Assessment of Combustion and Exhaust Emissions in a Common-Rail Diesel Engine Fueled With Methane and Hydrogen/Methane Mixtures Under Different Compression Ratio," Int. J. Hydrogen Energy, **45**(4), pp. 3263–3283.
[20] Jha, P. R., Wijeyakulasuriya, S., Krishnan, S. R., and Srinivasan, K. K., 2022, "Numerical Investigations of Low Load Diesel-Methane Dual Fuel Combustion at Early Diesel Injection Timings," Fuel, **315**, p. 123077.
[21] Hockett, A., Hampson, G., and Marchese, A. J., 2016, "Development and Validation of a Reduced Chemical Kinetic Mechanism for Computational Fluid Dynamics Simulations of Natural Gas/Diesel Dual-Fuel Engines," Energy Fuels, **30**(3), pp. 2414–2427.
[22] Li, Y., Li, H., Guo, H., Li, Y., and Yao, M., 2017, "A Numerical Investigation on Methane Combustion and Emissions From a Natural Gas-Diesel Dual Fuel Engine Using CFD Model," Appl. Energy, **205**, pp. 153–162.
[23] Huang, J., Hill, P. G., Bushe, W. K., and Munshi, S. R., 2004, "Shock-Tube Study of Methane Ignition Under Engine-Relevant Conditions: Experiments and Modeling," Combust. Flame, **136**(1–2), pp. 25–42.
[24] Burke, U., Somers, K. P., O'Toole, P., Zinner, C. M., Marquet, N., Bourque, G., Petersen, E. L., Metcalfe, W. K., Serinyel, Z., and Curran, H. J., 2015, "An Ignition Delay and Kinetic Modeling Study of Methane, Dimethyl Ether, and Their Mixtures at High Pressures," Combust. Flame, **162**(2), pp. 315–330.
[25] El-Sabor Mohamed, A. A., Panigrahy, S., Sahu, A. B., Bourque, G., and Curran, H. J., 2021, "An Experimental and Kinetic Modeling Study of the Auto-Ignition of Natural Gas Blends Containing C1–C7 Alkanes," Proc. Combust. Inst., **38**(1), pp. 365–373.
[26] Zhang, K., Banyon, C., Bugler, J., Curran, H. J., Rodriguez, A., Herbinet, O., Battin-Leclerc, F., B'Chir, C., and Heufer, K. A., 2016, "An Updated Experimental and Kinetic Modeling Study of n-Heptane Oxidation," Combust. Flame, **172**, pp. 116–135.
[27] Yu, L., Wang, S., Wang, W., Qiu, Y., Qian, Y., Mao, Y., and Lu, X., 2019, "Exploration of Chemical Composition Effects on the Autoignition of Two Commercial Diesels: Rapid Compression Machine Experiments and Model Simulation," Combust. Flame, **204**, pp. 204–219.
[28] Liang, J., Zhang, Z., Li, G., Wan, Q., Xu, L., and Fan, S., 2019, "Experimental and Kinetic Studies of Ignition Processes of the Methane–n-Heptane Mixtures," Fuel, **235**, pp. 522–529.
[29] Schuh, S., Ramalingam, A. K., Minwegen, H., Heufer, K. A., and Winter, F., 2019, "Experimental Investigation and Benchmark Study of Oxidation of Methane–Propane–n-Heptane Mixtures at Pressures Up to 100 Bar," Energies, **12**(18), p. 3410.
[30] Gong, Z., Feng, L., Qu, W., Li, L., and Wei, L., 2020, "Auto-Ignition Characteristics of Methane/n-Heptane Mixtures Under Carbon Dioxide and Water Dilution Conditions," Appl. Energy, **278**, p. 115639.
[31] Zhu, J., Li, J., Wang, S., Raza, M., Qian, Y., Feng, Y., Yu, L., Mao, Y., and Lu, X., 2021, "Ignition Delay Time Measurements and Kinetic Modeling of Methane/Diesel Mixtures at Elevated Pressures," Combust. Flame, **229**, p. 111390.
[32] Wu, Y. T., Yang, M., Tang, C. L., Liu, Y., Zhang, P., and Huang, Z. H., 2019, "Promoting "Adiabatic Core" Approximation in a Rapid Compression Machine by an Optimized Creviced Piston Design," Fuel, **251**, pp. 328–340.
[33] Liu, Y., Tang, C. L., Zhan, C., Wu, Y. T., Yang, M., and Huang, Z. H., 2019, "Low Temperature Auto-Ignition Characteristics of Methylcyclohexane/Ethanol Blend Fuels: Ignition Delay Time Measurement and Kinetic Analysis," Energy, **177**, pp. 465–475.
[34] Yang, M., Yang, Y., Liao, C., Tang, C., Zhou, C.-W., and Huang, Z., 2020, "The Auto-Ignition Boundary of Ethylene/Nitrous Oxide as a Promising Monopropellant," Combust. Flame, **221**, pp. 64–73.
[35] Mittal, G., and Sung, C. J., 2007, "A Rapid Compression Machine for Chemical Kinetics Studies at Elevated Pressures and Temperatures," Combust. Sci. Technol., **179**(3), pp. 497–530.
[36] Weber, B. W., Sung, C.-J., and Renfro, M. W., 2015, "On the Uncertainty of Temperature Estimation in a Rapid Compression Machine," Combust. Flame, **162**(6), pp. 2518–2528.
[37] Sung, C. J., and Curran, H. J., 2014, "Using Rapid Compression Machines for Chemical Kinetics Studies," Prog. Energy Combust. Sci., **44**, pp. 1–18.
[38] ANSYS, Inc., 2023, *ANSYS CHEMKIN-Pro® Academic Research, Release 18.2*, ANSYS, Inc., Canonsburg, PA.
[39] Mehl, M., Pitz, W. J., Westbrook, C. K., and Curran, H. J., 2011, "Kinetic Modeling of Gasoline Surrogate Components and Mixtures Under Engine Conditions," Proc. Combust. Inst., **33**(1), pp. 193–200.
[40] Wu, Y., Panigrahy, S., Sahu, A. B., Bariki, C., Beeckmann, J., Liang, J., Mohamed, A. A. E., Dong, S., Tang, C., Pitsch, H., Huang, Z., and Curran, H. J., 2021, "Understanding the Antagonistic Effect of Methanol as a Component in Surrogate Fuel Models: A Case Study of Methanol/n-Heptane Mixtures," Combust. Flame, **226**, pp. 229–242.
[41] Loparo, Z. E., Lopez, J. G., Neupane, S., Partridge, W. P., Vodopyanov, K., and Vasu, S. S., 2017, "Fuel-Rich n-Heptane Oxidation: A Shock Tube and Laser Absorption Study," Combust. Flame, **185**, pp. 220–233.
[42] Gong, Z., Feng, L. Y., Wei, L., Qu, W. J., and Li, L. C., 2020, "Shock Tube and Kinetic Study on Ignition Characteristics of Lean Methane/n-Heptane Mixtures at Low and Elevated Pressures," Energy, **197**, p. 117242.
[43] Molana, M., Goyal, T., and Samimi-Abianeh, O., 2021, "Measurement and Simulation of n-Heptane Mixture Autoignition," Ind. Eng. Chem. Res., **60**(38), pp. 13859–13868.
[44] Zhang, Z., Zhao, H., Cao, L., Li, G., and Ju, Y., 2018, "Kinetic Effects of n-Heptane Addition on Low and High Temperature Oxidation of Methane in a Jet-Stirred Reactor," Energy Fuels, **32**(11), pp. 11970–11978.
[45] Song, C., Liang, J., Zhang, Z., Li, G., and Zhang, C., 2022, "Interpretation of Role of Methane in Low-Temperature Oxidation Processes of Methane/n-Heptane Mixtures," Fuel, **328**, p. 125373.
[46] Thorsen, L. S., Thestrup Jensen, M. S., Pullich, M. S., Christensen, J. M., Hashemi, H., and Glarborg, P., 2023, "Oxidation of Methane/n-Heptane Mixtures in a High-Pressure Flow Reactor," Energy Fuels, **37**(4), pp. 3048–3055.
[47] Kaczmarek, D., Atakan, B., and Kasper, T., 2019, "Investigation of the Partial Oxidation of Methane/n-Heptane-Mixtures and the Interaction of Methane and n-Heptane Under Ultra-Rich Conditions," Combust. Flame, **205**, pp. 345–357.
[48] Huang, J., and Bushe, W. K., 2006, "Experimental and Kinetic Study of Autoignition in Methane/Ethane/Air and Methane/Propane/Air Mixtures Under Engine-Relevant Conditions," Combust. Flame, **144**(1–2), pp. 74–88.
[49] Uygun, Y., Ishihara, S., and Olivier, H., 2014, "A High Pressure Ignition Delay Time Study of 2-Methylfuran and Tetrahydrofuran in Shock Tubes," Combust. Flame, **161**(10), pp. 2519–2530.
[50] Zhang, P., Zsély, I. G., Samu, V., Nagy, T., and Turányi, T., 2021, "Comparison of Methane Combustion Mechanisms Using Shock Tube and Rapid Compression Machine Ignition Delay Time Measurements," Energy Fuels, **35**(15), pp. 12329–12351.
[51] Ramalingam, A., Zhang, K., Dhongde, A., Virnich, L., Sankhla, H., Curran, H., and Heufer, A., 2017, "An RCM Experimental and Modeling Study on CH4 and CH4/C2H6 Oxidation at Pressures Up to 160 Bar," Fuel, **206**, pp. 325–333.
[52] Lightfoot, P. D., Roussel, P., Caralp, F., and Lesclaux, R., 1991, "Flash Photolysis Study of the CH_3O_2+ CH_3O_2 and CH_3O_2+ HO_2 Reactions Between 600 and 719 K: Unimolecular Decomposition of Methylhydroperoxide," J. Chem. Soc. Faraday Trans., **87**(19), p. 3213.
[53] Anglada, J. M., Olivella, S., and Sole, A., 2006, "Mechanistic Study of the CH(3)O (2)(*) + HO(2)(*) –> CH(3)O(2)H + O(2) Reaction in the Gas Phase. computational Evidence for the Formation of a Hydrogen-Bonded Diradical Complex," J. Phys. Chem. A, **110**(18), pp. 6073–6082.
[54] Tsang, W., and Hampson, R. F., 1986, "Chemical Kinetic Data Base for Combustion Chemistry. Part I. Methane and Related Compounds," J. Phys. Chem. Ref. Data, **15**(3), pp. 1087–1279.
[55] Westbrook, C. K., 2000, "Chemical Kinetics of Hydrocarbon Ignition in Practical Combustion Systems," Proc. Combust. Inst., **28**(2), pp. 1563–1577.